



Quantifying microcracks on fractured bone surfaces – Potential use in forensic anthropology

Steven J. Walden^{a,*}, Wendy Rowe^b, Jacqui Mulville^c, Sam L. Evans^d, Peter Zioupos^e

^a School of Engineering, School of History, Archaeology and Religion, Cardiff University, UK

^b School of Dentistry, Cardiff University, UK

^c School of History, Archaeology and Religion, Cardiff University, UK

^d School of Engineering, Cardiff University, UK

^e School of Engineering, University of Hull, UK

ARTICLE INFO

Keywords:

Forensic archaeology/anthropology

Bone microcracks

Scanning-electron-microscopy (SEM)

ABSTRACT

Bone fracture surface morphology (FSM) can provide valuable information on the cause of failure in forensic and archaeological applications and it depends primarily on three factors, the loading conditions (like strain rate), the ambient conditions (wet or dry bone material) and the quality of bone material itself. The quality of bone material evidently changes in taphonomy as a result of the decomposition process and that in turn is expected to affect FSM. Porcine bones were fractured by a standardised impact during the course of soft tissue decomposition, at 28-day intervals, over 140 days (equivalent to 638 cooling degree days). Measurements of the associated microcracks on the fractured cortical bone surfaces indicated a progressive increase in mean length during decomposition from around 180 μm –375 μm . The morphology of these microcracks also altered, from multiple intersecting microcracks emanating from a central point at 0–28 cumulative cooling degree days, to longer linear cracks appearing to track lamellae as soft tissue decomposition progressed. The implications of these findings are that taphonomic changes of bone may offer the real possibility of distinguishing perimortem and taphonomic damage and also provide a new surrogate parameter for estimation of post-mortem interval (PMI) in forensics.

1. Introduction

Bone fracture surface morphology (FSM) depends primarily on three factors, the loading conditions (like strain rate), the ambient conditions (wet or dry bone material) and the quality of bone material itself (Zioupos et al., 2000). The quality of bone material evidently changes in taphonomy as a result to the decomposition process and that in turn is expected to affect FSM. Fractography is a powerful tool for deciphering the events associated with the creation and progress of fracture (Piekariski, 1970; Zioupos, 1999; Gupta and Zioupos, 2008). In the forensic context it may be able to distinguish between ante-, peri- and post-mortem trauma with obvious benefits in medicolegal research and practice. The present study focused on the presence and characteristics of microcracks on fractured cortical bone surfaces and examined whether they vary during the course of soft tissue putrefaction, and if so, whether they could offer an indication of when the fracture occurred. Such changes could help to distinguish between perimortem and post-mortem trauma in cortical bone in forensic and archaeological

applications. Microcracks in this context are defined as microscopic cracks less than 1 mm in length. This choice is based on measurements in the literature that critical size defects in bone are of this order of magnitude, of which the average size of a microcrack is $\sim 360 \mu\text{m}$ and the plastic zone size ahead of it another $\sim 170\text{--}200 \mu\text{m}$ (Robertson et al., 1978).

Gross morphological characteristics of perimortem cortical bone trauma are currently believed to include sharp, jagged edges, the presence of fracture lines, and smooth (as opposed to rough textured or fibrous) surfaces of fractured bone (Wheatley, 2008). In forensic cases, these characteristics are still currently examined in the context of known fracture typology to determine possible aetiologies: sharp force (cut marks/kerfs); blunt force (crushed/impacted bone); penetrating versus non-penetrating wound etc. (Ubelaker et al., 1997) Many taphonomic processes can also alter bone, some of which directly or indirectly cause post-mortem bone damage resulting in fracture and/or disarticulation. Human intervention (intentional or unintentional) may contribute to such damage. In forensic and archaeological contexts, this brings to the

* Corresponding author.

E-mail address: steve.walden@southwales.ac.uk (S.J. Walden).

<https://doi.org/10.1016/j.jmbbm.2023.105824>

Received 2 July 2022; Received in revised form 17 March 2023; Accepted 1 April 2023

Available online 3 April 2023

1751-6161/© 2023 The Authors. Published by Elsevier Ltd. This is an open access article under the CC BY-NC-ND license (<http://creativecommons.org/licenses/by-nc-nd/4.0/>).

foreground the importance of distinguishing perimortem fracture due to assault, from post-mortem taphonomic damage which may mimic it^{2 6 7}.

Other methods that use fracture characteristics to understand the timing of bone damage include the Fracture Freshness Index (Karr and Outram, 2012) (Karr and Outram, 2012). The method, employed in archaeological studies, defines three principal criteria of fracture (pertaining to long bones): angle (criterion A); outline (B); and edge texture (C) are criteria widely used because they can be applied to all long bone fragments and provide a rapid and simple method^{3 8}. For each criterion, a score of zero, one or two is used to describe each fragment. Zero is scored if the fracture fragment was entirely consistent with fresh or perimortem damage. One would be scored if some 'unfresh' features were present and two would be scored if 'unfresh' features dominated. To create the index value for a given fragment, the scores for the three criteria are summed. This gives an index ranging from zero to six. Zero indicates a specimen entirely consistent with fresh fracture and six indicates a specimen that lacks almost all fresh fracture features.

Karr and Outram's fracture freshness index is arguably best suited towards the use for which it was developed i.e., the analysis of bone subject to butchery for consumption of marrow. The method does not lend itself to quantifiable data to allow inferential statistical analysis. There is also a risk when generalising these assessment criteria to cortical bone fragments not originating from long bones. This has some implications for robust archaeological analysis of fractured cortical bone, but more so for analysis in the forensic context, wherein the probabilistic interpretation of such scientific data must be seen to be implemented for said data to be acceptable as expert testimony in a court of law. There are microstructural correlates that are equally indicative of perimortem cortical bone trauma and demonstrate progressive change during decomposition. From these changes, novel quantifiable metrics like microcrack length, angle of intersection, density etc. Can be obtained which could lend themselves more readily than the current subjective interpretation of gross morphological characteristics that pervade the literature, to subsequent inferential Bayesian statistical analysis required to meet evidential standards for the court. The value of this novel approach in the forensic context can thus be argued on this point.

Other potential applications of the present research exist for archaeological investigations (battlefield trauma, sacrificial practices, comparative analysis of suspected perimortem trauma in early hominids, etc.) as well in forensic investigations contributing to providing insight into the cultures of the past, and providing closure for the bereft in the present.

Osteonal cortical bone can be modelled at the micromechanical level as a solid resembling a fibre-reinforced composite as posited by Currey (2003) (Currey, 2003), Najafi et al. (2007) (Najafi et al., 2007), and others. Osteons consist themselves of 10–30 concentric lamellae (fibrous layers of bone) of between 3 and 7 μm thickness, surrounding a fluid filled Haversian canal containing one or two capillaries and nerve fibres. The osteon is separated from surrounding incoherent interstitial bone by a thin amorphous layer, the cement line (Currey, 2003). When a bone cracks due to applied force, a stress field develops along the end of the main cracks as a function of crack length, location, loading and geometry. The heterogeneous structure of bone (Rho et al., 1998) allows microcracks to initiate ahead of the main crack and also forces the main crack to branch deviate and deflect off its course. As we know these toughening mechanisms reduce the stress intensity at the tip of the main crack and make it less likely to propagate. Microcracks (Najafi et al., 2007; Rho et al., 1998; O'Brien et al., 2005) develop in this context in the various bone pockets of various tissue ages, mineral contents and architectures that constitute this highly variable, hybrid, heterogeneous, composite and hierarchical organisation of bone^{10 12 13 14}.

Microscopic examination of fracture surfaces using scanning electron microscopy (SEM) revealed the complexity of bone changes (Shipman et al., 1981). While the fracture surfaces of fresh bone appear smooth macroscopically, it was found that perimortem fractures appeared

roughened and fibrous microscopically. The reason for this microscopic appearance is that the fracture front either follows the predominant direction of mineralized collagen bundles or breaks the bonds between adjacent bundles. Fractures of dry bone will have a roughened and stepped appearance both macroscopically and microscopically because the fracture front perpendicularly intersects the collagen bundles (Shipman et al., 1981).

As the elasticity, strength and toughness of fresh and dry bone differ, it is reasonable to consider that microcracking of fractured surfaces would show a difference over time^{10 8}. During decomposition of soft tissue, it is possible that the tissue fluid in Haversian canals is replaced to an extent (at least in close proximity to perimortem and/or taphonomic bone damage) by putrefaction fluid due to capillary action (a variable mixture of cellular and tissue residues and complex fatty acids bathing the bone) (Charlier et al., 2008). Further to this, Hollund et al. (2012) noted that humic staining and pyrite inclusions indicate that fleshed remains were interred early post-mortem in a low-oxygen and humic-rich environment, which they believed may have inhibited further bacterial tunnelling (Holland et al., 2012). Finally, they posited that an increase in oxygen levels possibly due to cross-cutting ditches and/or lowering of groundwater levels contributed to the oxidation of pyrite followed by acidification, generalised destruction, micro-fissures and staining by iron oxide compounds indicating a change in the burial conditions. Critically this infers that a microenvironment seems to have been created within the middle of the bones.

As decomposition progresses (assuming surface deposition or shallow burial of remains in a temperate climate), putrefaction fluid seeps away and/or evaporates, proteins and other organic components lyse, and bone progressively dries (Najafi et al., 2007). These organic changes and dehydration may progressively affect the mechanical properties of bone during soft tissue decomposition. To test this a standardised impact trauma was applied at 28-day intervals during soft tissue putrefaction to fracture bone, with the cogent changes in microcracking, visible on fracture surfaces, examined under SEM^{18 19}. To test the effects of putrefaction fluid ingress, porcine bone samples were immersed in progressively stronger molarities of stearic acid for the same period of time as the putrefaction experiment to approximate these conditions and observe the effects on fracture surface morphology under SEM. Returning to the mechanical properties of porcine bone regarding fracture, porcine bone has been noted as similar to human bone in this respect (Seil et al., 1998) (Seil et al., 1998). Whilst canid bone has been argued by some to have greater similarity to human bone still in these respects, it is not readily available whereas porcine bone can be readily obtained. Whereas canid status as a companion animal is likely to encounter rejection on ethical grounds if posited as an animal model for forensic science experimentation as here, no such stigma is ascribed to porcine bone as the animals are already farmed for human consumption (Aerssens et al., 1998) (Aerssens et al., 1998). Porcine ribs were selected as this facilitated both larger experimental sample sizes relative to available materials, and they did not require being cut into beams for the experiment, promoting experimental validity and authenticity in the forensic context respectively.

2. Materials and methods

Scanning electron microscopy can be used to quantify different modes of single, parallel, and crosshatched cracks (as demonstrated in electron micrographs, Fig. 2). To determine if certain combinations of such cracks are specific to perimortem bone trauma and/or a specific point in soft tissue decomposition time since deposition, prevailing temperatures and known deposition conditions were correlated with progressive changes in microcrack morphology. This was achieved by using porcine bone samples, retrieved from surface and shallow burial depositions at monthly intervals and impacting them using a standardised test method and then examining the resultant microcracks on fractured bones surfaces under SEM. Polyvinylsiloxane® casts were

made of microcracks on fractured surfaces of archaeological bone for comparison (see below).

Fresh bone samples (ribs) were obtained from pigs killed within the previous 24 h at an abattoir. Soft tissue was debulked to leave a layer of between 20 mm and 50 mm of muscle tissue over the bone and was frozen for a period of not less than 48 h at $-20\text{ }^{\circ}\text{C}$ (Seil et al., 1998). The purpose of the freezing was dual fold, firstly to facilitate easier machine cutting of bone samples, secondly to negate the effects of friction generated heat when machine cutting and thus minimising thermal damage. The bones were then machined into 20 mm thick transverse section samples with a Draper 100 W band saw at low speed. The samples were defrosted and further debulked to leave a layer of soft tissue 20 mm thick around the cortical bone, as an approximation of average human pectoral/intercostal muscle tissue (Aerssens et al., 1998). These samples were then impacted from a drop height of 200 mm, with a custom hemi-cylindrical tup of 15 mm radius and 100 mm width, attached to a 5 kg drop weight on a calibrated Instron Dynatup® impact tester. This method of impact was chosen to emulate blunt force trauma in a potential assault scenario as authentically as possible whilst allowing for standardised measurement. Samples were supported on a flat plate beneath. The ribs fractured mainly along the longitudinal axis; occasionally transverse fractures occurred.

Twenty samples were broken immediately upon defrosting and acted as the T0 perimortem analogue for the surface deposition group and shallow burial (300 mm depth) groups, and intrinsic experimental control. A further 50 samples were left intact initially. These samples were placed under a porous layer of 30 μm micro-mesh membrane before being covered in a 50 mm deep layer of leaf litter (simulated with bark chips for uniformity), to facilitate decomposition via microbial action, and water perfusion whilst preventing more severe taphonomic damage to the samples. Ten samples were removed and fractured at four weekly intervals over a period of six months (T0–T140 days) to act as a post-mortem surface deposition group.

For the shallow group a further fifty samples were similarly left intact and decomposed at a depth of 300 mm below loam soil (25 L total) in an aerated 1000 mm (l) by 200 mm (w) by 330 mm (d) trough, pH 6.5, placed under a porous layer of 30 μm micro-mesh membrane before being buried, to facilitate decomposition via microbial action, and water perfusion whilst preventing more severe taphonomic damage to the samples, spanning the same period of six months. Again, groups of 10 of these were removed and fractured at 28-day intervals.

All samples, once buried, or deposited on the surface, were locked in a cage (originally a rabbit run), tethered to posts at the corners to deter scavengers. Cumulative cooling degree-days were calculated to provide standardised comparison. Degree days are calculated by taking the difference between the daily temperature mean, (high temperature plus low temperature divided by two) and $4\text{ }^{\circ}\text{C}$ selected as the base temperature. If the temperature mean is above $4\text{ }^{\circ}\text{C}$, we subtract $4\text{ }^{\circ}\text{C}$ from the mean and the result is Cooling Degree Days (CDD). This standard was chosen as decomposition occurs more readily above $4\text{ }^{\circ}\text{C}$, and took place during spring and early summer in the UK. Lower winter temperatures ($4\text{ }^{\circ}\text{C}$ or less) would have slowed or potentially arrested decomposition (see Table 1 for conversions).

Cooling degree days are a measure of how much (in degrees), and for how long (in days), the outside air temperature was above a certain level. For this study it is indicative of all days during the measured soft tissue putrefaction period(s) where temperature is above $4\text{ }^{\circ}\text{C}$ and thus

within the temperature range of active microbial decomposition, and enzymolysis. Where D_d is the daily (cooling) degree-days for one day, \varnothing_b is the base temperature and $\varnothing_{0,j}$ is the outdoor temperature in hour j , the value is calculated as follows. The subscript denotes that only positive values are taken (Turpin, 2017).

$$D = \sum_{j=1}^{24} (\varnothing_b - \varnothing_{0,j}) ((\varnothing_b - \varnothing_{0,j}) > 0) / 24 \quad (\text{Eq. 1})$$

After fracturing, all porcine experimental bone samples were first freeze dried in a Thermo® Heto PowerDry model PL3000 freeze dryer at $-50\text{ }^{\circ}\text{C}$ at an atmospheric pressure of 2 Pa, for 96 h. Once dried the samples were gold sputtered (to facilitate conductivity) in a Peltier cooled Emi Tech model K675X, to a depth of 48 nm. It has been noted by Turpin et al. (2017) (Turpin, 2017) that osteonal microcracks are more likely to occur with rapid freezing treatments, so whilst an artefact due to freeze drying cannot be entirely discounted, it would be unlikely with the technique use here. The fractured surfaces of the samples were then examined at 13–16 times magnification and 14 keV beam intensity using a SEM Tech EBT1 scanning electron microscope, to determine changes in microcrack morphology in cortical bone during the decomposition process. For the stearic acid experiment to replicate putrefaction fluid ingress into bone, previously fractured porcine rib samples were soaked at $25\text{ }^{\circ}\text{C}$ for 56 days (nodular appearance occurred at 56 days decomposition, equating to 82 cumulative cooling degree days) in progressively stronger concentrations of stearic acid in ethanol: Pure ethanol (negative control); 0.16M stearic acid in ethanol; 1.0M stearic acid in ethanol; and finally, 10.0M stearic acid in ethanol (high concentration, acting as a positive control).

3. Results

The mean length of microcracks, observed on the cortical fracture surfaces of the experimental porcine rib fragments, demonstrated an upward trend as soft tissue putrefaction progressed (see Fig. 1). Electron micrographs illustrating the difference between microcrack lengths at the outset and completion of soft tissue putrefaction are shown in Fig. 2. Following the application of Levene's test to verify the non-parametric nature of the data to be tested, sequential paired Mann-Whitney U testing showed some statistically significant increases in microcrack length on the fracture surfaces of the porcine experimental rib fragments between 28 and 82 cumulative cooling degree days' (CCDD) decomposition, as well as statistically significant differences between surface and burial deposition scenarios (see Table 2).

For the porcine samples, in both surface and burial deposition scenarios, the mean length of the microcracks on fractured cortical bone surfaces inflicted by the standardised impact progressively increased from approximately 180 μm –375 μm during soft tissue decomposition, over 140 days in situ, equating to 638 cooling degree days in total. The morphology of these microcracks altered from multiple intersecting cracks (conglomerates of three microcracks emanating from a central point) at 0–28 cumulative cooling degree days to longer linear cracks, appearing to track lamellae as soft tissue decomposition progressed. Statistically, significantly greater increase was shown in microcrack length in the first 12 weeks of decomposition in the surface deposition scenario as compared to the burial deposition scenario, which suggests any changes affecting the structural and mechanical characteristics of

Table 1
Conversion Table Outlining Cooling Degree days for the Soft Tissue Putrefaction Period.

Chronological Days Conversion to Cooling Degree Days for this period ($4\text{ }^{\circ}\text{C}$ base temperature).					
T0	T28	T56	T84	T112	T140
0	28	82	183	422	638
Cumulative cooling degree days	cumulative cooling degree days	cumulative cooling degree days	cumulative cooling degree days	cumulative cooling degree days	cumulative cooling degree days

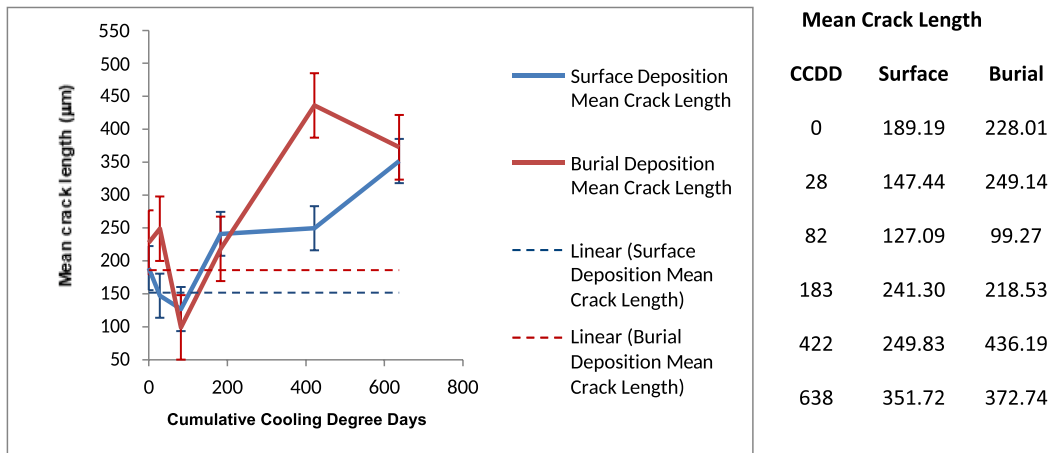


Fig. 1. Upward trend in microcrack length on fractured bone surfaces during soft tissue putrefaction. Standard error is shown (± standard error), n = 25 to 471, depending on number of cracks visible in the visual fields selected for each parameter.

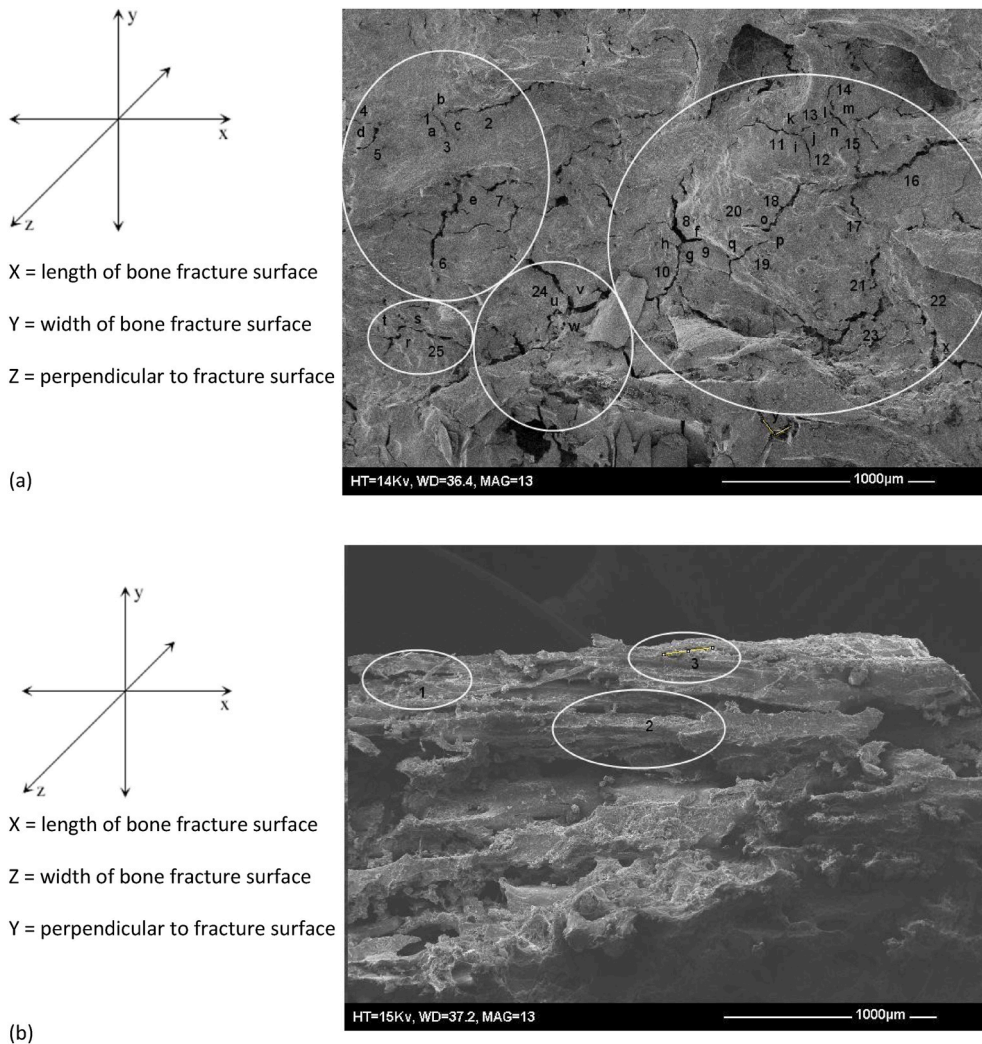


Fig. 2. Electron micrographs of fractured experimental porcine bone surfaces: (a) T0 (0 cumulative cooling days decomposition); (b) T140 (638 cumulative cooling days decomposition). In both cases microcracks are numbered, and angles of intersection are lettered.

the bone were taking place more quickly in the former. Features believed due to acidic etching by putrefaction fluid (pitting of porcine cortical bone surfaces, nodular features in remaining transitional and/or trabecular bone), were evident primarily in bone samples fractured at 82

cumulative cooling degree days in surface and burial deposition scenarios (Fig. 4). These features were less evident at 183 cumulative degree days.

Table 2
Inferential Statistics re: Sequential Microcrack Length Change.

Parameters	Levene's Test: Ho ² Normal Data Distribution, reject if p <0.05. Accept or reject Ho ²	Mann- Whitney p- Value	Ho Null Hypothesis: No difference in micro- crack length. Bonferroni corrected α = 0.01 Accept or reject Ho ²
Group 1: Surface Deposition Sequential Pairs			
1. T0 Vs T28 Micro-crack Length Surface Deposition	p = 0.36, cannot reject H0.	0.45	Accept null hypothesis.
2. T28 Vs T56 Micro-crack Length Surface Deposition	p = 0.00, reject H0.	0.00	Reject null hypothesis.
3. T56 Vs T84 Micro-crack Length Surface Deposition	p = 0.00, reject H0.	0.00	Reject null hypothesis.
4. T84 Vs T112 Micro-crack Length Surface Deposition	p = 0.24, cannot reject H0.	0.00	Reject null hypothesis.
5. T112 Vs T140 Micro-crack Length Surface Deposition	p = 0.95, cannot reject H0.	0.14	Accept null hypothesis.
Group 2: Burial Deposition Sequential Pairs			
1. T0 Vs T28 Micro-crack Length Burial Deposition	p = 0.06, cannot reject H0.	0.08	Accept null hypothesis.
2. T28 Vs T56 Micro-crack Length Burial Deposition	p = 0.87, cannot reject H0.	0.07	Accept null hypothesis.
3. T56 Vs T84 Micro-crack Length Burial Deposition	p = 0.00, reject H0.	0.00	Reject null hypothesis.
4. T84 Vs T112 Micro-crack Length Burial Deposition	p = 0.98, cannot reject H0.	0.42	Accept null hypothesis.
5. T112 Vs T140 Micro-crack Length Burial Deposition	p = 0.24, cannot reject H0.	0.08	Accept null hypothesis.
Group 3: Surface Vs Burial Deposition Corresponding Pairs			
1. T0 Surface Deposition Vs T0 Burial Deposition Microcrack Length	p = 0.01, reject H0.	0.00	Reject null hypothesis.
2. T28 Surface Deposition Vs T28 Burial Deposition Microcrack Length	p = 0.01, reject H0.	0.00	Reject null hypothesis.
3. T56 Surface Deposition Vs T56 Burial Deposition Microcrack Length	p = 0.05, cannot reject H0.	0.00	Reject null hypothesis.
4. T84 Surface Deposition Vs T84 Burial Deposition Microcrack Length	p = 0.59, cannot reject H0.	0.91	Accept null hypothesis.
5. T112 Surface Deposition Vs T112 Burial Deposition Microcrack Length	p = 0.58, cannot reject H0.	0.01	Reject null hypothesis.
6. T140 Surface Deposition Vs T140 Burial Deposition Microcrack Length	p = 0.63, cannot reject H0.	0.77	Accept null hypothesis.

4. Discussion

Changes in microcrack morphology resulting from standardised blunt force trauma during soft tissue decomposition can be considered indicative of cogent changes in the structural and mechanical characteristics of the experimental porcine cortical bone samples. The bone material they are made of resembles in architecture a fibre reinforced composite and contains osteons that contain tissue fluid. The fluid may

be replaced by putrefaction fluid under capillary action as soft tissue decomposition progresses. The osteon lumen then becomes either an empty channel or one occluded by precipitated putrefaction fluid residues as water is progressively lost (Najafi et al., 2007; Child, 1995). The cement line around an osteon according to Burr et al. (1988) (Burr et al., 1988) is partly demineralised compared to surrounding cortical bone, it contains sulphated mucoids and is also likely to be lost as decomposition progresses (De Troyer et al., 2003). The literature shows that microcracks deviate around osteons when they meet the cement line, and if the cement line is preferentially damaged then cracks will propagate further (see Fig. 3). Najafi et al. (2007) posited that this deviation reduces as the elastic modulus of osteons decreases, which occurs when the osteon and/or cement line softens^{5 10}. This may arguably be the case in a dehydrated osteon where sulphated mucoids have been lost from the cement line. This provides a possible mechanism for the increase in microcrack length observed as decomposition progresses: the fibre reinforcement effect of the bone composite in structural terms was progressively lost, so microcrack trajectory was less impeded as the stress field (damage zone) spread from the point where impact was applied on the porcine bone samples. Collagen fibre density in cortical bone is lowest in the interstitial 'seams' between concentric lamellar layers, and could according to research by Reznikov et al. (2013), be comparatively less mineralized in these regions (Reznikov et al., 2013). Collagen would be dissipated further as it lyses during progressive decomposition, decreasing structural integrity, providing a further path of least resistance to propagating microcracks^{5 8}. This may explain why they seem more likely to track between lamellar layers in cortical bone as decomposition progresses. Collagen is one of the two main ingredients of the composite nature of bone, the organic phase, which imparts stability at fracture, increased toughness and cohesion to the bone material. Collagen degradation will affect the toughness of bone directly (Zioupou et al., 1999), (Zioupou, 2001). Toughness being achieved through the ability to sustain microcracks and generate microcracks as opposed to larger deleterious cracks implies a direct relation between collagen degradation, collagen impairment and microcrack density.

As decomposition progressed there was an increase in net length of microcracks on the fractured cortical bone surfaces in both burial and surface deposition scenarios (Fig. 1). Whilst there was a general upward trend in this regard, there was variation between individual data points with increases and decreases in microcrack length, which is likely due to intrinsic variations between individual bones as whilst similar, no two will be entirely uniform in composition. There was also a change in morphology from intersecting conglomerates of three cracks emanating from a point, to a more linear format. It has already been mentioned that in fresh bone, the Haversian canals at the centre of osteons are filled with tissue fluid which may well be replaced with putrefaction fluid (at least in bone damaged by trauma) by capillary action during the early stages of soft tissue putrefaction. Fluid filled osteons and their associated networks of canaliculi, having a lower relative density compared to surrounding cortical bone, may provide a focal point for the stress field, spreading from the large crack tip emanating from a point of impact. To refer to Kasiri and Taylor (2008) (Kasiri and Taylor, 2008), failure, such as a microcrack, is predicted to occur if the stress applied (such as blunt force trauma) exceeds a critical value at a certain distance, from a notch (read osteons and associated canaliculi in the context of this research) (Kasiri and Taylor, 2008).

Microcracks are generated and distributed widely in bone and with relation to the various heterogeneous packets of bone tissue in it. They are also in relation to the load magnitude which varies locally and with respect to the distance from stress concentrating features such as the notch of a major fracture crack or architectural features such pores, cavities or vessels. The length of the microcracks on the fresh and 28 CCDD decomposition porcine bone fracture surfaces were less than 0.4 mm and appear to radiate from a central point. The microcracks became longer and more linear from 82 CCDD decomposition onward. As the

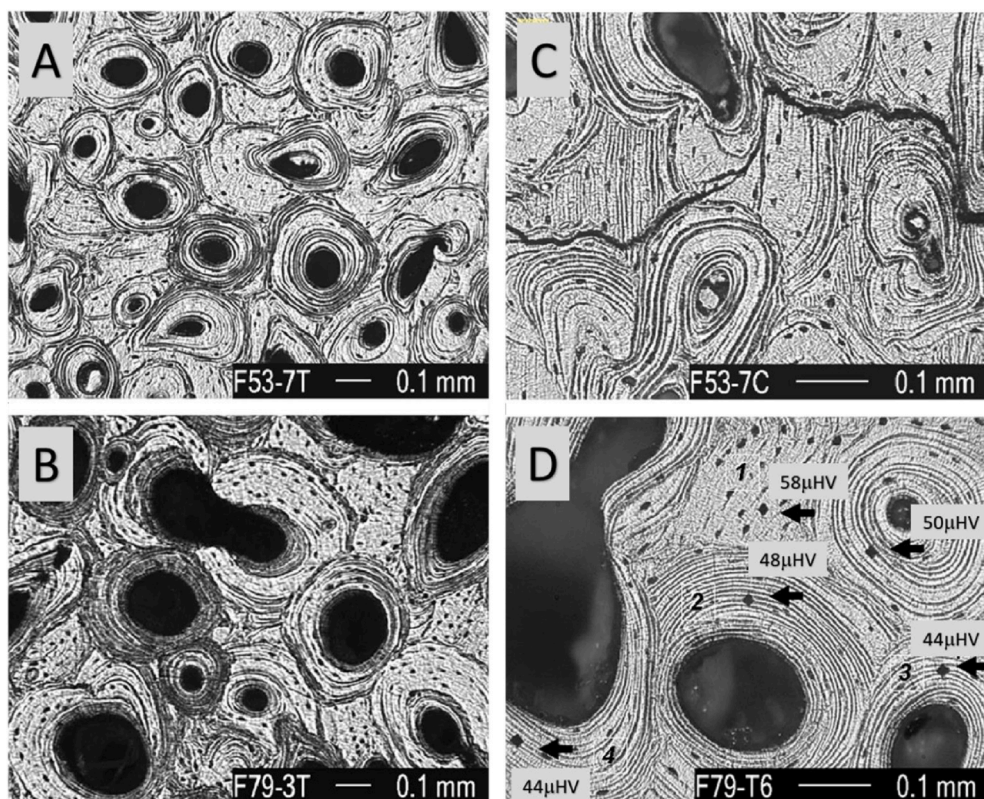


Fig. 3. Micrographs of histological cross sections of human bone tissue from a previous study which demonstrate the highly heterogeneous and variable structure of bone tissue at this level. This changes considerably in life as shown (A) for a 53yr old and (B) 79yr old female. (C) when a major crack grows, it deflects and meanders between the various architectural packets following the lines of elastic mismatch, which are demonstrated in (D) by the Vickers microhardness values at each point (low values in osteons and high in interstitial lamellae). (Original photos from (Kasiri and Taylor, 2008) annotated for the present figure).

(concentrations of) osteons, and notably the Haversian canals and canalicular networks they contain, become progressively more occluded with comparatively denser precipitated putrefaction residues (Najafi et al., 2007; Holland et al., 2012; Kuhn et al., 2007) and possibly materials from the deposition matrix, the stress concentration effect may become mitigated. From a mechanical perspective the bone becomes structurally more homogenous, cogently altering the trajectory of propagating microcracks resulting from any applied force (Seil et al., 1998; Robertson et al., 1978; Karr and Outram, 2012). As decomposition progresses, collagen and water are lost from the bone, so toughness and the critical distance parameter may also vary.

There are some limitations in the present study and further research is warranted on certain topics. If concentrations of osteons are the foci of the microcracks, they are likely to have been substantially damaged or obliterated in the porcine samples from 28 days decomposition onward with putrefaction fluid ingress, resultant acidification, and its eventual precipitation potentially contributing to this process. To examine the mechanisms posited in the discussion above further, controlled microcracking and examination (under high magnification SEM) of individual osteons, in experimental porcine bone samples at 28-day intervals from fresh through to 140 days decomposition (the period of soft tissue decomposition) should be considered. This should include all skeletal elements to ascertain anatomical variations. It should be noted that the above analyses and discussion are predicated on young adult porcine bone. The histomorphology of juvenile cortical bone varies from this, in particular with respect to osteonal density, which may be considerably less, by the order of 50%^{29, 30}. It should therefore be considered that microcracks resulting from the same standardised blunt force impact may have a different morphology in decomposing juvenile bone. Other factors may also have an effect and should be accounted for. For instance, there is the confounding effects of the combination of type of bone and the kind of standardised exogenous force application. Bone originating from older individuals, pathological bone, or thermally or chemically modified bone, may show differing microcrack morphologies, and, variations of the externally applied force (direction,

magnitude, strain rates etc.) may combine to give a greater variety of outcomes.

It is worth noting that relatively lower magnifications ($\times 13$ – 16 times) used with the scanning electron microscope allowed the survey of wider areas of the fracture surfaces whilst providing reliable information and rapid results. From the forensic perspective this could enable a rapid yet reliable survey of suspect bone trauma in the evidential context as part of a time limited investigation.

In conclusion, from the data obtained, the observed changes in microcrack morphology on fractured bone surfaces subsequent to blunt force trauma, cannot in isolation be used as a perimortem trauma indicator. These changes only became more readily apparent after 28 cumulative cooling degree days, particularly in the surface deposition scenario. However, the changes in microcrack morphology do appear to be time related with regards to a progressive decomposition of soft tissue and possibly the bone itself. It must be noted that this experiment should be replicated with other skeletal elements to determine if results can be generalised – the greater thickness of cortical bone in long bones for instance would likely affect microcrack propagation. Therefore, there is potential for this method to be utilised in the forensic context to link SEM identified bone trauma to the earliest phases of decomposition, inclusive of the possibility of perimortem bone trauma. There is also the possibility that with further refinement of the method the time since death (post-mortem interval) estimation may be improved. The appearance of features from damage by putrefaction fluids (described earlier) will also limit the timescale within which the fracture occurred (i.e., before the putrefaction fluids dried out).

Ethics

Ethical approval was not required as tissue samples were obtained from animals already butchered for human consumption.

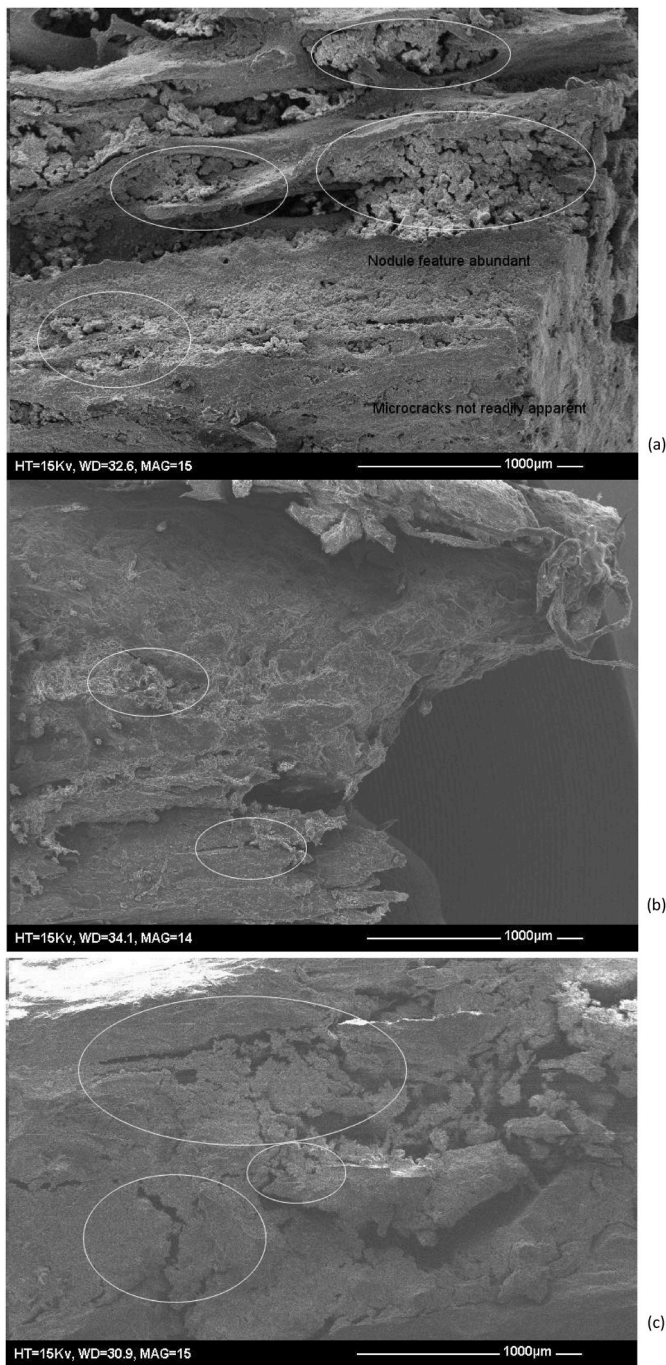


Fig. 4. Comparison of Features Potentially due to Acidic Putrefaction Fluid Ingress (Nodular features circled): (a) T56 82 CCDD Porcine Bone; (b) T56 Days Stearic Acid 0.16M; (c) T56 Days Stearic Acid 1.0M.

Funding

SJW was supported by a Cardiff University (Self-Funded PGR Studies).

Research data sharing and availability

Open Access (Cardiff University Repository).

CRedit authorship contribution statement

Steven J. Walden: Methodology, Investigation, Formal analysis,

Conceptualization. Wendy Rowe: Methodology, Investigation, Formal analysis, Data curation. Jacqui Mulville: Supervision, Methodology, Formal analysis. Sam L. Evans: Supervision, Methodology, Investigation, Formal analysis, Conceptualization. Peter Zioupos: Writing – review & editing, Methodology, Formal analysis.

Declaration of competing interest

The authors declare that they have no known competing financial interests or personal relationships that could have appeared to influence the work reported in this paper.

Data availability

The authors are unable or have chosen not to specify which data has been used.

Acknowledgments

GM Short, Butchers Llanhilleth (supplied all porcine tissue).

References

- Aerrens, J., Boonen, S., Lowet, G., Dequeker, J., 1998. Interspecies differences in bone composition, density, and quality: potential implications for in vivo bone research. *Endocrinology* 139 (2), 663–670.
- Burr, D.B., Schaffler, M.B., Frederickson, R.G., 1988. Composition of the cement line and its possible mechanical role as a local interface in human compact. *Bone*” J. Biomechanics 11, 939–945.
- Charlier, P., Georges, P., Bouchet, F., Huynh-Charlier, I., Brun, L., Blondiaux, J., Grandmaison, G.L., 2008. The microscopic (optical and SEM) examination of putrefaction fluid deposits (PFD). Potential interest in forensic anthropology. *Virchows Arch.* 453, 377–386.
- Child, A.M., 1995. Towards an understanding of the microbial decomposition of archaeological bone in the burial environment. *J. Archaeol. Sci.* 22, 165–174.
- Currey, J.D., 2003. How well are bones designed to resist fracture? *J. Bone Miner. Res.* 18 (4), 591–598.
- De Troyer, A., Gorman, R.B., Gandevia, S.C., 2003. Distribution of inspiratory drive to the external intercostal muscles in humans. *J. Physiol.* 546 (3), 943–954.
- Gupta, H., Zioupos, P., 2008. Fracture of bone tissue: the ‘hows’ and the ‘whys. *Med. Eng. Phys.* 30 (10), 1209–1226.
- Holland, H.I., Jans, M.M.E., Collins, M.J., Kars, H., Joosten, I., Kars, S.M., 2012. What happened here? Bone histology as a tool in decoding the postmortem histories of archaeological bone from Castricum, The Netherlands. *Int. J. Osteoarchaeol.* 22 (5), 537–548.
- Karr, L.P., Outram, A.K., 2012. Tracking changes in bone fracture morphology over time: environment, taphonomy, and the archaeological record. *J. Archaeol. Sci.* 39 (2), 555–559.
- Kasiri, S., Taylor, D., 2008. A critical distance study of stress concentrations. *Bone*” J. Biomechanics 41, 603–609.
- Kuhn, G., Sultz, M., Muller, R., Ruhli, F.J., 2007. Diagnostic value of Micro-CT in comparison with histology in the qualitative assessment of historical human postcranial bone pathologies. *J. Comparat. Human Biol.* 58, 97–115.
- Najafi, A.R., Arshi, A.R., Elsami, M.R., Fariborz, S., Moeinzadeh, M.H., 2007. Micromechanics fracture in osteonal cortical bone: a study of the interactions between microcrack propagation, microstructure and the material properties. *J. Biomech.* 40, 2788–2795.
- O’Brien, F.J., Taylor, D., Lee, T.C., 2005. “The Effect of Bone Microstructure on the Initiation and Growth of Microcracks”. *J. Orthopaedic Res.* 23, 475–480.
- Piekarski, K., 1970. Fracture of bone. *J. Appl. Phys.* 41, 215. <https://doi.org/10.1063/1.1658323>.
- Reznikov, N., Almany-Magal, R., Weiner, S., 2013. Three-dimensional imaging of collagen fibril organization in rat circumferential lamellar bone using a dual beam electron microscope reveals ordered and disordered sub-lamellar Structures. *Bone* 52, 676–683.
- Rho, J.Y., Kuhn-Spearing, L., Zioupos, P., 1998. Mechanical properties and the hierarchical structure of bone. *Med. Eng. Phys.* 20 (2), 92–102.
- Robertson, D.M., Robertson, D., Barrett, C.R., 1978. Fracture toughness, critical crack length and plastic zone size in bone. *J. Biomech.* 11 (8–9), 359–364.
- Seil, R., Rupp, S., Krauss, P.W., Benz, A., Kohn, D.M., 1998. Comparison of initial fixation strength between biodegradable and metallic interference screws and a press-fit fixation technique in a porcine model. *Am. J. Sports Med.* 26 (6), 815–819.
- Shipman, P., Johnson, A.J., Stahl, S., 1981. Hydraulic behavior of bones and the fossil record. *January Am. J. Phys. Anthropol.* 54 (2), 277 (Abstract).
- Turpin, C., 2017. The micro-taphonomy of cold: differential microcracking in response to experimental cold-stresses. *J. Forensic Sci.* 62 (5), 1134–1139.
- Ubelaker, D.H., 1997. Taphonomic applications in forensic anthropology. In: Haglund, W.D., Sorg, M.H. (Eds.), *Forensic Taphonomy: the Postmortem Fate of Human Remains*. CRC Press, pp. pp77–90.

- Wheatley, B.P., 2008. Perimortem or Postmortem Bone Fractures? An experimental study of fracture patterns in deer femora. *J. Forensic Sci.* 53 (1), 69–72.
- Zioupos, P., 1999. Recent developments in the study of failure of solid biomaterials and bone: 'Fracture' and 'pre-fracture' toughness. *Mater. Sci. Eng. C: Mater. Biol. Applic.* 6 (1), 33–40.
- Zioupos, P., 2001. Ageing Human Bone: factors affecting its biomechanical properties and the role of collagen. *J. Biomater. Appl.* 15 (3), 187–229.
- Zioupos, P., Currey, J.D., Hamer, A.J., 1999. The role of collagen in the declining mechanical properties of aging human cortical bone. *J. Biomed. Mater. Res.* 45 (2), 108–116.
- Zioupos, P., Smith, C.W., An, Y.H., 2000. Factors affecting mechanical properties of bone. In: An, Y.H., Draughn, R.A. (Eds.), *Mechanical Testing of Bone and the Bone-Implant Interface*, Chap.4. CRC Press, Boca Raton, USA, pp. 65–85.